Magnetic handshake materials as a scale-invariant platform for programmed self-assembly

Ran Niu[a,1], Chrisy Xiyu Du[b], Edward Esposito[a], Jakin Ng[a], Michael P. Brenner[b], Paul L. McEuen[a,c], and Itai Cohen[a,c,1]

[a]Laboratory of Atomic and Solid State Physics, Cornell University, Ithaca, NY 14853; [b]School of Engineering and Applied Sciences, Harvard University, Cambridge, MA 02139; and [c]Kavli Institute at Cornell for Nanoscale Science, Cornell University, Ithaca, NY 14853

Edited by John A. Rogers, Northwestern University, Evanston, IL, and approved October 24, 2019 (received for review June 16, 2019)

Programmable self-assembly of smart, digital, and structurally complex materials from simple components at size scales from the macro to the nano remains a long-standing goal of material science. Here, we introduce a platform based on magnetic encoding of information to drive programmable self-assembly that works across length scales. Our building blocks consist of panels with different patterns of magnetic dipoles that are capable of specific binding. Because the ratios of the different panel-binding energies are scale-invariant, this approach can, in principle, be applied down to the nanometer scale. Using a centimeter-sized version of these panels, we demonstrate 3 canonical hallmarks of assembly: controlled polymerization of individual building blocks; assembly of 1-dimensional strands made of panels connected by elastic backbones into secondary structures; and hierarchical assembly of 2-dimensional nets into 3-dimensional objects. We envision that magnetic encoding of assembly instructions into primary structures of panels, strands, and nets will lead to the formation of secondary and even tertiary structures that transmit information, act as mechanical elements, or function as machines on scales ranging from the nano to the macro.

magnetic handshake material | information encoding | specific interaction | programmable self-assembly

Programmable self-assembly of complex arrangements from simple units requires encoding local interaction rules into building blocks to select a desired final structure. At the microscale and nanoscale, such rules have been encoded through entropic and enthalpic interactions (1–3). For example, previous work has shown that entropic bonds arising from particle shape alone can lead to formation of complex crystal structures (3–5). Other pioneering studies incorporated enthalpic interactions through DNA-mediated colloidal (2, 6–12) and DNA origami/Lego self-assembly platforms (13–18). These latter strategies have been successful at generating complex structures ranging from clathrate colloidal crystals (19) to complex polyhedra and nanoscale DNA teddy bears (14). Despite tremendous successes achieved by these pioneering studies, these binding strategies typically only function at small size scales and often suffer from long annealing times, as elements must diffuse into near contact to interact (20, 21). Moreover, the resulting materials are inherently soft since thermal fluctuations are necessary for these systems to explore their phase space and arrive at optimal binding configurations. To develop complementary platforms that overcome such challenges at the microscale and nanoscale, it is necessary to develop strategies based on building blocks that encode binding interactions that are both stronger and longer-ranged.

At the macroscale, pioneering studies and even some toys have used enthalpic interactions based on magnetic dipole forces to assemble 3-dimensional (3D) structures (22–24). Such forces are long-ranged and strong enough to direct assembly, but, to date, only the simplest dipole configurations have been explored, and the programmable potential of this approach to assembly is largely untapped.

Here, we propose an assembly platform based on encoding magnetic information into panels that is powerful, general, and can be applied across length scales. These panels are composed of a magnetically patterned layer with an array of magnets capped on either side by spacers (see, for example, Fig. 1*A*). The binding specificity and energy of the panels depend on the magnetic dipole patterns. Since the ratio of the binding energies depends only on the design, key aspects of this platform are scale-invariant down to dimensions as small as ~ 10 nm, below which magnetic domains become unstable due to thermal fluctuations.

To demonstrate the feasibility of our approach, we show that a macroscale version of this platform can achieve controlled polymerization, assemblies reminiscent of those that are attained by DNA strands, and the folding of 2-dimensional (2D) nets into 3D structures. For simplicity, we demonstrate our approach using a 2×2 array of magnets oriented parallel to the magnetic layer axis, which results in 4 unique patterns that we color-code as shown in Fig 1*A*. Spacers were glued to the magnetically patterned layers to enhance selectivity of the panel interactions, as shown in Fig. 1*B*. The resulting panels are 0.90 cm in diameter and 0.64 cm thick. We find that when placed on a flat frictional mylar surface, matched panels will spontaneously bind, even when the face-to-face separation is larger than the panel thickness. The range for spontaneous binding increases even further when panels are agitated on a shaker table to overcome

Significance

Programmable self-assembly of smart, digital, and structurally complex materials from simple components remains a long-standing goal of material science. Here, we propose an assembly platform where information is encoded into building blocks using arrays of magnets that induce specific binding. Similar to current state-of-the-art platforms, magnetic encoding can achieve controlled polymerization of lone panels, complementary binding of panel strands, and 3D assembly of panel nets. This platform, however, has several advantages over current methods in that the approach is scale-invariant, has tunable mechanical strength, and has high information capacity for programmable self-assembly. We envision that this approach will lead to the formation of structures that transmit information, act as mechanical elements, or function as machines across length scales.

Author contributions: R.N., C.X.D., E.E., M.P.B., P.L.M., and I.C. designed research; R.N., C.X.D., and J.N. performed research; M.P.B. contributed new reagents/analytic tools; R.N. and C.X.D. analyzed data; and R.N., C.X.D., E.E., and I.C. wrote the paper.

The authors declare no competing interest.

This article is a PNAS Direct Submission.

[1]To whom correspondence may be addressed. Email: rn362@cornell.edu or ic64@cornell.edu.

This article contains supporting information online at https://www.pnas.org/lookup/suppl/doi:10.1073/pnas.1910332116/-/DCSupplemental.

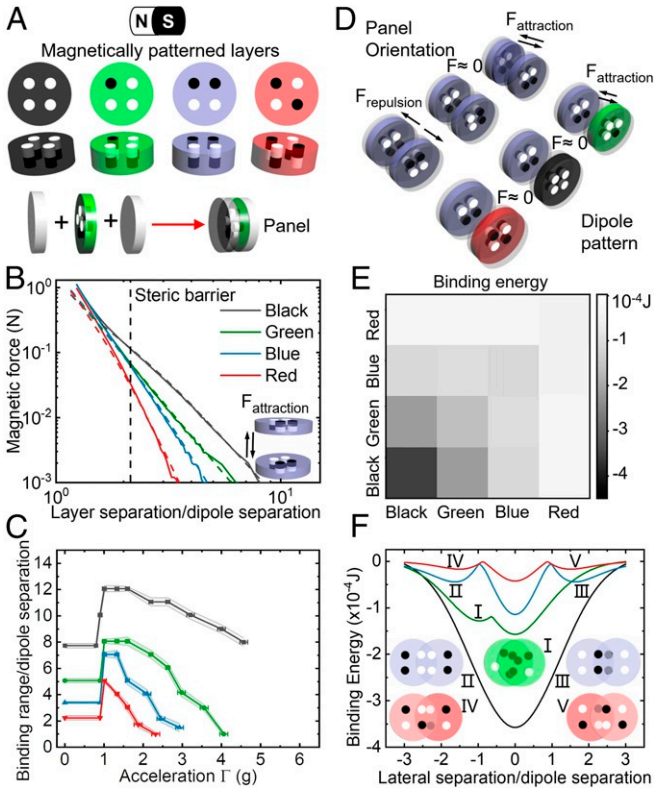

Fig. 1. Encoding information into magnetic panels to generate specific interactions. (*A*) Four unique magnetically patterned layers are constructed by using a 2×2 array of magnets with different orientations (top and side views). The magnetically patterned layers are arbitrarily colored black, green, blue, and red according to their dipole patterns. Spacers are glued to the 2 faces of the magnetically patterned layer to make a panel. (*B*) Magnetic force between 2 magnetically patterned layers of the same pattern at the optimal binding orientation (sketch in *Inset*) versus the center-to-center layer separation. Here, we normalize the separation by the lateral dipole separation within a magnetically patterned layer. Solid lines are experimental measurements, and dashed lines are results from analytic calculations in which interactions between any 2 pairs of magnets that are not in the same magnetically patterned layer are considered. We glue spacers onto the magnetically patterned layers to further enhance the selectivity of the panel interactions. These spacers create a steric repulsion at a surface separation corresponding to the vertical dashed line. (*C*) Plot of the range for spontaneous binding (normalized by the dipole separation within a panel) versus Γ, the shaking acceleration normalized by g. Data are obtained by placing panels face to face, releasing them and determining if they spontaneously bind. (*D*) Schematic illustrating the interactions between panels of different orientations (top left) and dipole patterns (bottom right). (*E*) Theoretical calculation of the ground-state binding energy between any 2 panels. (*F*) Theoretical calculation of the binding-energy landscape of 2 panels of the same dipole pattern as a function of the lateral separation normalized by the dipole separation within a panel. The globally optimal ground state occurs when the panels are face to face with no separation. In addition, we find the metastable states of green, blue, and red panels. Data are obtained by orienting panels face to face with the separation equal to twice the spacer thickness. Energies are calculated by displacing the panels laterally, keeping the panels parallel, and optimizing their relative orientation in the panel plane.

friction. This range is maximal when the acceleration Γ, measured in units of the gravitational acceleration g, is just above 1. Further increase in Γ reduces the range for spontaneous binding, as panels are jostled into orientations unfavorable for binding (Fig. 1*C*). At high enough accelerations, the magnetic bonds break. More generally, the shaker can be thought of as providing an effective energy scale that plays a role similar to $k_B T$ in thermal systems (see *SI Appendix* for a more detailed discussion). Face-to-face interactions between panels depend both on the panel orientation and the dipole pattern (Fig. 1*D*), which results in an ordered hierarchy of binding interaction strengths. We calculate the binding energy between panels to determine the hierarchy of interactions for different panel combinations (Fig. 1*E*). We find that panels bind most strongly to their counterparts, with the exception of the green panels, which bind more strongly to the black panels. In addition to the global minimum, which occurs when the dipole patterns are aligned, we find metastable binding states for the green, blue, and red panels when they are translated laterally (Fig. 1*F*). This hierarchy of interactions allows for controlling the order of the assembly by varying Γ relative to the different panel binding strengths.

The ability to select the binding sequence opens the door to hierarchical polymerization, where successive panels attach in a specific order. To demonstrate this capability, we create Janus panels with a different binding strength at each surface by gluing 2 different magnetically patterned layers and spacers face to face (Fig. 2 *A*, *i*). There are 13 unique Janus panels arising from the different color-coded combinations of the dipole patterns (Fig. 2 *A*, *ii*), as well as the reversed dipole patterns that result from flipping the black and green layers over. The polymer assembly is controlled by the combination of Janus panels chosen. The polymerization proceeds by loading the panels onto the shaker table at high Γ. As Γ is lowered, for the different combinations of panels, we observe successive binding (Movies S1–S3) into dimers (Fig. 2 *A*, *iii*–*v*), trimers (Fig. 2 *A*, *iv* and *v*), hexamers (Fig. 2 *A*, *v*), and, finally, polymers whose assembly is determined by the hierarchy of binding interactions. In addition, as in colloidal and polymeric materials (25, 26), seeding the system with a branching nucleus allows for controlling the resulting topology (Fig. 2 *B*, *i* and *ii* and Movie S4). Further, by controlling the dipole pattern on the faces of the seed, we can control the growth sequence to create hybrid branched polymers (Fig. 2 *B*, *iii*). Thus, the specificity of the binding interactions determines the assembled structure, while the long-range nature of the interactions allows for directed assembly (Movies S1–S4). Looking forward, one could easily expand this approach to investigate more complex dipole patterns, the phase behavior of the panels in 2D, and even assembly of periodic open networks in 3D.

Such panels can also be made to assemble in a more collective manner by gluing them to elastic backbones that form secondary structures. Here, in direct analogy to base pairs in DNA strands, the panel sequence allows for encoding information and guiding assembly. We find that the unbinding behavior of paired strands with increasing shaking acceleration, Γ, depends sensitively on the panel dipole pattern, number of panels on each strand, sequence of the panels, and ratio of the panel types (Fig. 3*A*). These results are analogous to the melting behavior of double-stranded DNA with the general trends that increasing the number of pairing elements and the ratio of strong to weak elements increases the melting temperature (27–29). The theoretically determined unbinding curves (dashed lines in Fig. 3 *A*, *i*–*iv*) are qualitatively consistent with experimental results (see detailed discussion in *SI Appendix*). By prescribing the distance between nearby panels on 1 strand, we can generate bending of the secondary structure to form S shapes (Fig. 3 *B*, *i* and *ii* and Movie S5). Alternatively, we can design the panel sequence to include unpaired panels and make hairpins (Fig. 3 *B*, *iii* and Movie S5). By controlling the panel orientation relative to the backbone, we can generate twist and control the pitch of the secondary structure by the rotation angle of panels (Fig. 3 *C*, *i*–*iii* and Movie S5). In addition to these structural motifs, magnetic handshake strands can also be used to perform a toehold exchange, a type of strand displacement used in DNA to detect sequences, make molecular machines, and perform basic logic computations

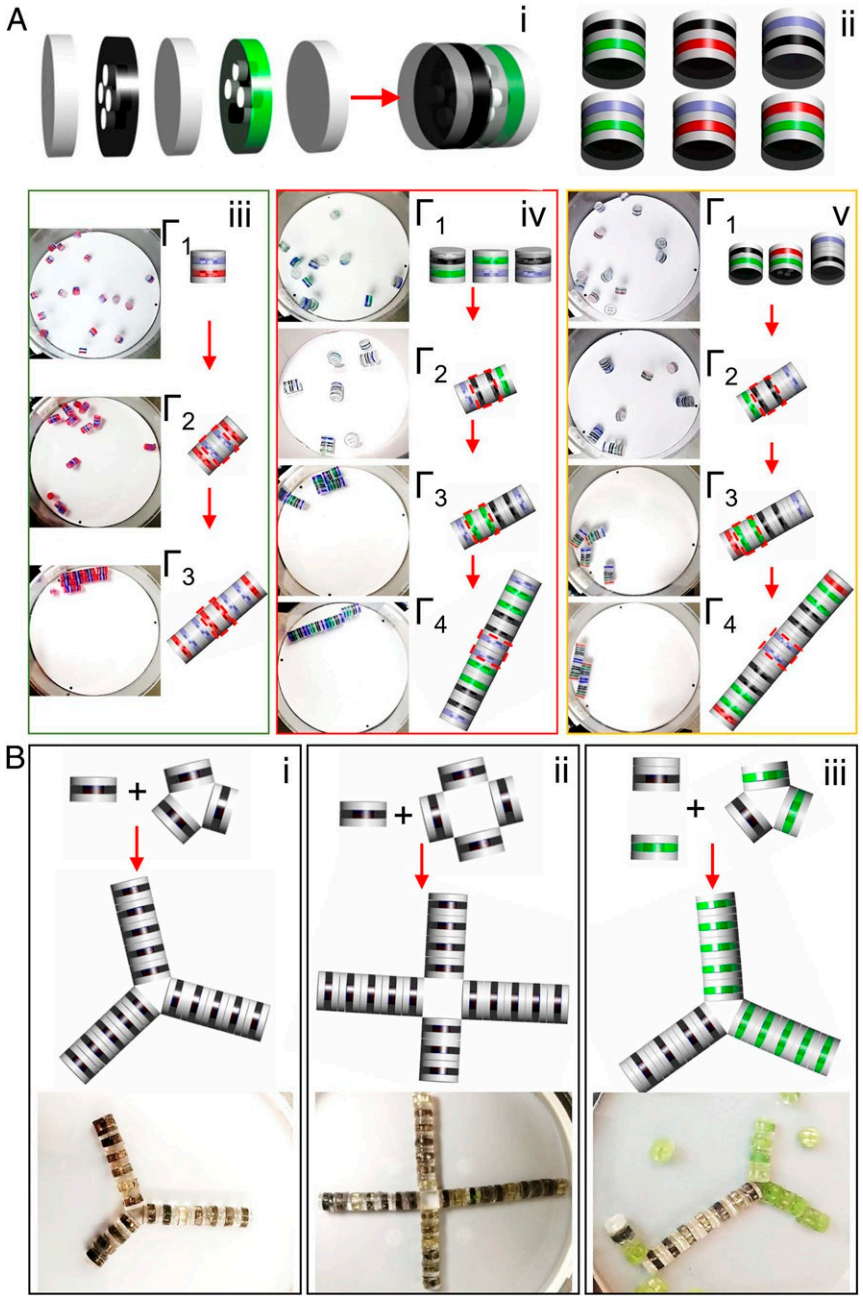

Fig. 2. Using Janus panels and structured seeds to control polymerization. (*A*) We control the polymerization sequence using Janus panels. (*A*, *i*) Janus panels are constructed from 2 different magnetically patterned layers and spacers, all of which are glued face to face. (*A*, *ii*) There are 6 color combinations. Since the 2 faces of the black and green layers are different from each other, Janus panels containing a single black or green magnetically patterned layer have 2 different possible combinations. The Janus panels containing both a green and a black magnetically patterned layer have 4 different possible combinations. Thus, there are 13 possible Janus panels that can be constructed from magnetically patterned layers with the 2×2 dipole array. (*A*, *iii*–*v*) We show 3 different schemes for controlling the polymerization sequence of Janus panels. (*A*, *iii*) Blue/red Janus panels self-assemble into dimers at $\Gamma = 3.6g$ and longer polymers at $\Gamma = 2.4g$. (*A*, *iv*) Green/black, black/blue, and green/blue Janus panels form dimers at $\Gamma = 6.5g$, trimers at $\Gamma = 3.9g$, and long polymers at $\Gamma = 3.0g$. Interestingly, we find that for the black/blue Janus panel, the black layer interferes with the binding of the blue layer. Therefore, these blue panels can only bind to blue panels from green/blue Janus panels. (*A*, *v*) Green/black, black/blue, and green/red Janus panels self-assemble into dimers at $\Gamma = 6.8g$, trimers at $\Gamma = 4.3g$, and hexamers at $\Gamma = 3.0g$. Here, we add 2 extra spacers in the blue/black Janus panel to permit binding of blue panels to one another. (*B*) We use structured seeds to control polymer topology. (*B*, *i* and *ii*) We use 3- and 4-faced seeds to grow 3-branched (*B*, *i*) and 4-branched (*B*, *ii*) polymers made of black panels. (*B*, *iii*) We use a 3-faced hybrid seed to grow a 3-branched hybrid polymer with 2 green branches and 1 black branch.

(30–32). Here, a complementary but short strand is displaced with another complementary but longer strand. When the toehold region has the same binding energy as the rest of the panels in the strand, a minimum of 2 panels is needed for the toehold exchange. If the toehold region consists of panels with sufficiently stronger binding than those in the rest of the strand (as is the case for black toehold panels on an otherwise green strand; Fig. 3 *D*, *i*–*iv* and Movie S5), a single panel is sufficient for the toehold exchange. These demonstrations suggest that many of the design principles developed for DNA information storage, assembly, and computation can be directly ported over to magnetic handshake strands.

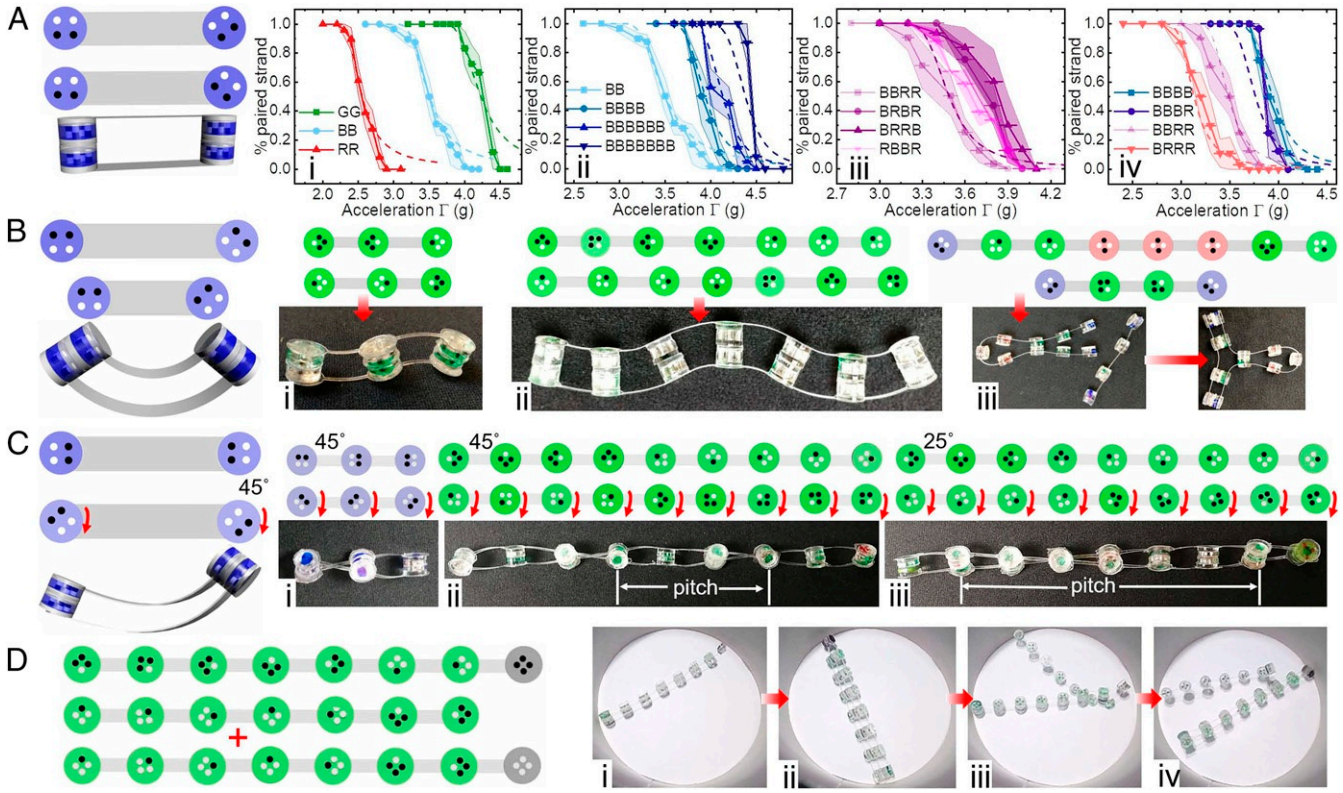

Fig. 3. Magnetic strands and the resulting secondary structures. We make flat (*A*), bent (*B*), and twisted (*C*) structures from 2 complementary strands. (*A*) Percent of paired strands at different Γ is sensitive to panel dipole pattern (*i*), number of pairing panels (*ii*), panel sequence (*iii*), and red-to-blue panel ratio (*iv*). The keys indicate the panel sequence and length. The shaded regions indicate the SE from 5 independent experimental measurements. The dashed lines are obtained from theoretical calculations. The broadening in the low probability region at high Γ is expected since the experiment consists of measurements on a small number of paired strands (see *SI Appendix* for details). (*B*) Bending structures: shortest S-shaped strand (*i*), long S-shaped strand (*ii*), and hairpin structure (*iii*). (*C*) We create twisted structures by rotating the panels in 1 strand relative to the backbone (red arrows). (*C*, *i*) Shortest helix. (*C*, *ii* and *iii*) We control the pitch of the helices by changing the rotation angle of the panels from 45° in *ii* to 25° in *iii*. (*D*) Toehold exchange of a short complementary strand with a longer complementary strand. Here, spacers are used to weaken binding on 1 side of each strand. Initially, only the toehold region is exposed and available for strong binding. The leftmost panel shows a schematic of the initial pair of strands and the added longer strand (indicated by the +). (*D*, *i*–*iv*) Images from a movie of the toehold exchange. In snapshot *D*, *i*, we show the initial pair of strands. In snapshot *D*, *ii*, we show that the added longer complementary strand binds to both the toehold region and weakly to the other pair of strands. Such complexes do not have analogues in DNA. In *D*, *iii*, we observe that only the toehold region of the long chain, which consists of a single black panel, remains bound. Finally, in snapshot *D*, *iv*, the short strand is completely displaced by the long strand, completing the toehold exchange.

One can dramatically increase the design complexity to guide assembly and make mechanically stronger structures by placing panels on 2D elastic backbones. Here, the panel choice, arrangement, orientation, and spacing, as well as the net architecture, can all be varied to robustly assemble a desired final configuration. We show 4 examples of 3D structures that assemble hierarchically from pairs of such nets in Fig. 4 (and Movie S6). Panels with different binding strengths were used to determine the order of assembly as Γ is decreased. In addition, the panel orientation (engineering designs in the 1st column of Fig. 4, with enlarged schemes in *SI Appendix*) was used to ensure proper alignment and handedness of the 2 nets (first column of photographs in Fig. 4). We carefully chose the backbone bending energy and segment length for each net so that under agitation, they can bend out of the plane and form bonds that sustain the 3D structure (2nd column of photographs in Fig. 4). Finally, the weakest-binding panels were used to lock the structures into place and complete the assembly (last column in Fig. 4). Crucially, through combining these design strategies, we were able to bypass the many metastable configurations that arise when the panel-binding sequence is uncontrolled (Movie S6). Avoiding these metastable structures allowed for assembly of these macroscale structures within minutes (Movie S7). These examples illustrate the potential for building hierarchically complex structures and the need for further development of systematic approaches for implementing these strategies.

As designs become more sophisticated, these building blocks could be made to assemble into structures that act as messengers, serve as mechanical elements in metamaterials, or function as machines. The magnetic moments of the panels allow for using external magnetic fields to facilitate assembly, disassemble undesired configurations, and, at lower field strengths, actuate the assemblies in complex environments (33–35). Such capabilities highlight the high degree of control that is available in the assembly and function of magnetic handshake materials, which is a great advance over macroscale assembly platforms that only use 1 or 2 magnetic dipole interactions and are agnostic to sequence (22–24).

Intriguingly, there have been several new technological developments in the fabrication and alignment of nanoscale magnetic domains, as well as the fabrication of nanometer-thick elastic materials that indicate that our platform could be reproduced at the microscale and nanoscale. The smallest scale at which materials can maintain stable magnetization is determined by the superparamagnetic limit, when the magnetic energy is comparable to the thermal energy. The magnetic energy of a domain scales as $N\mu_B B$, where N is the number of atoms in a cubic

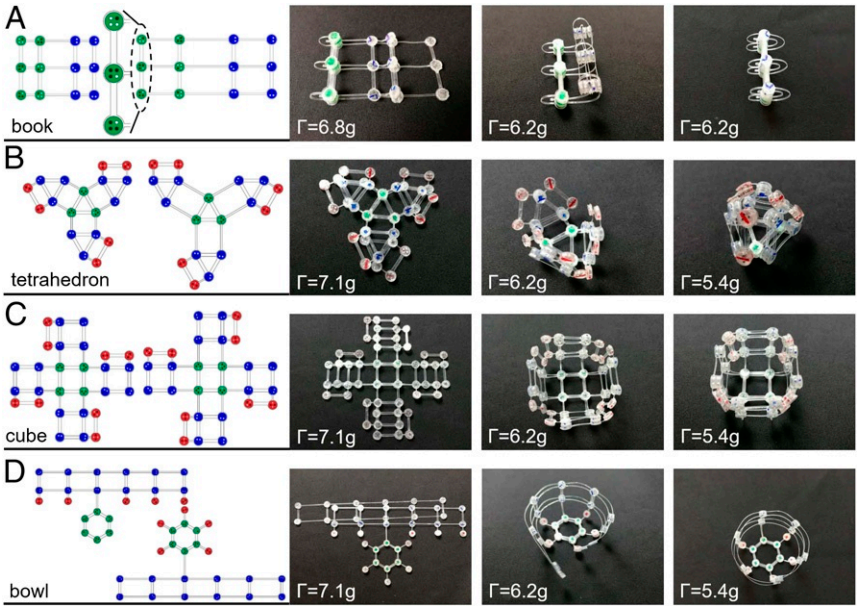

Fig. 4. Hierarchical self-assembly of 2D nets into 3D structures. Using the different binding energies of the different panels, their orientation, as well as the width, length, and thickness of the 2D net elements, we assemble various 3D structures: a book (*A*), a tetrahedron (*B*), a cube (*C*), and a bowl (*D*). In the leftmost column, we show the engineering design for each pair of nets. We vary the width of the net elements so that some elements bend and others remain flat. In addition, to enhance selectivity of the binding, we vary the panel orientations relative to the nets: enlarged regions in *A*. To assemble the final structures, we place the nets in our shaker apparatus at random locations. For the shaking amplitudes we can achieve in our apparatus, the acceleration is not sufficient to completely flip the nets over. We therefore place the nets with the appropriate face-up or face-down orientation. We start the assembly at high Γ and show still images at various points in the assembly as Γ is decreased.

magnetic material, $\mu_B \approx 0.06$ meV/T is the Bohr magneton, and $B = \mu_0 H_c \sim 10^{-2}$ T is a typical coercive field for common ferromagnets. This energy becomes comparable to $k_B T$ when a magnetic domain contains $N = 4.3 \times 10^4$ atoms which would yield a cube ~10 nm on a side. Thus, as magnetic storage technology continues to miniaturize (36, 37), our panels could, in principle, be fabricated to be ~30 nm in lateral dimension and ~10 nm in height, comparable to many state-of-the-art systems for nanocolloid assembly (38). For 2 such contacting domains, the binding energy, given by $V(r) = -\mu_0 (N\mu_B)^2 / 2\pi r^3$, is 3.2×10^{-20} J or $\sim 8 k_B T$ at room temperature. Increased spacing between panels via deposition of spacer layers, eliminating van der Waals interactions using steric repulsion layers (39, 40), as well as increasing binding strength using depletion interactions (41, 42) or cDNA strands (2, 6) would then enable further tuning of the binding energy relative to $k_B T$. Additionally, it has been demonstrated that 2-nm-thick elastic backbone materials can be fabricated via atomic layer deposition (43). Using these materials, features as small as 200 nm could be patterned by using photolithographic steppers, and features even as small as 6 nm could be patterned by using e-beam methods. These backbones would have a Young's modulus of tens to hundreds of

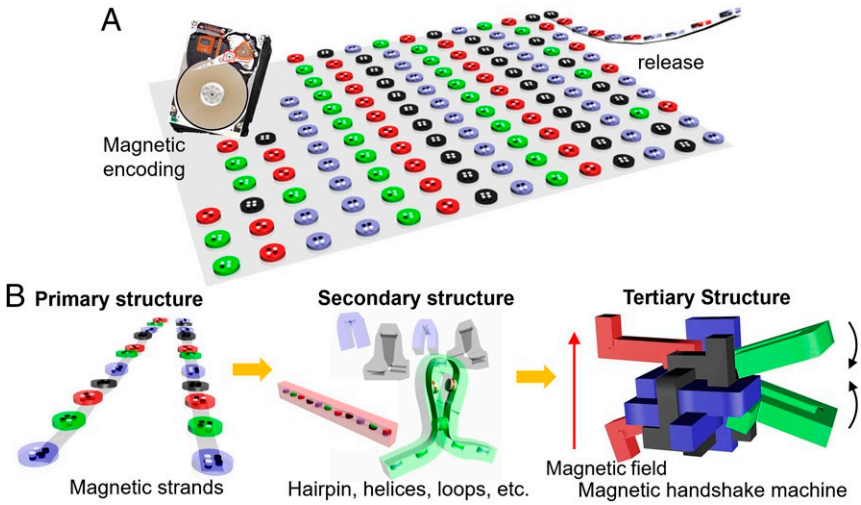

Fig. 5. Vision for assembly of magnetic handshake materials. (*A*) Magnetic recording and lithography create panels and strands on a wafer that are released after fabrication. (*B*) A strand's sequence or primary structure encodes information for secondary structure formation and self-assembly into a 3D magnetically actuated machine.

gigapascals and bending stiffness that is orders of magnitude higher than $k_B T$ (43). When combined with the magnetized panels, analogues of the building blocks we demonstrated in our macroscale studies could be fabricated to within a factor of 7 of these limits with currently available magnetic write technologies. Moreover, because both the magnetic and elastic energies scale with volume, the relative energetics governing assembly of these structures remains identical, independent of scale (43).

One can imagine various strategies for fabrication of these building blocks en masse at relatively little cost per structural/magnetic element. At the millimeter scale, recently developed magnetic 3D printing technologies (33) could be used to fabricate these elements. At even smaller scales, one could imagine one day loading a fabricated wafer into an apparatus similar to a modern hard drive and using a computer to write the desired dipole patterns. Upon release, the magnetized primary structures would self-assemble into microscale secondary structures, and even tertiary structures or machines that can be actuated using external magnetic fields (Fig. 5). Therefore, such fabrication methods could be used to unleash this powerful scale-invariant platform of magnetic handshake materials and advance the field of design.

Materials and Methods

Panel Design. Acrylic disks of diameter 0.90 cm and thickness 0.32 or 0.16 cm with 4 holes of diameter 0.16 cm and nearest separation 0.30 cm in the disk axis direction for inserting magnets were printed on a laser cutter (Zing 40 watt; Epilog Laser). Spacers of diameter 0.90 cm and thickness 0.16 or 0.025 cm were also printed on the laser cutter from a piece of acrylic sheet or Mylar. Cylindrical neodymium magnets (grade N48) of diameter 0.16 cm and height 0.32 cm or 0.16 cm (totalElement®) were inserted and glued into the holes of the acrylic disk according to the designed orientations.

Unbinding of Magnetic Strands. We initialized the experiments by putting all of the strands in pairing state in the sample cell. For comparison between different experiments, the number density of panels in our 2D sample cell (height of 1.7 times panel diameter) was kept to be the same. We started from low acceleration Γ and increased Γ stepwise at a rate of $(0.1-0.2)g/2min$ to make sure the number of unpaired strands did not change further with time at each Γ. The number of single strands was counted, and the fraction of single strands to the number of total strands was calculated. Each experiment was repeated 4 or 5 times to obtain a SE.

The theoretical unbinding curves of magnetic strands were obtained by analytical calculation of the probability of the pairing state as a function of temperature based on the partition function of the whole system. The partition function of the system was calculated based on careful accounting of the system's translational entropy, rotational entropy, and binding enthalpy.

More details of the experimental setup used for measurements, experimental design, and theoretical modeling are shown in *SI Appendix*. Data are available upon request.

ACKNOWLEDGMENTS. This work was supported by NSF Grant DMR-1435829, Defense Advanced Research Projects Agency Grant ARL FA8650-19-1-7914, and Cornell Center for Materials Research Grant DMR-1719875. M.P.B. and C.X.D. were supported by Office of Naval Research Grant N00014-17-1-3029. We thank Richard Liebert and Sloane Amato for help with the initial phase of the project, as well as Wei Wang, Kyle Dorsey, Tanner Pearson, Meera Ramaswamy, Ofer Kimchi, and Andrei Klishin for helpful discussions.

1. I. B. Liu, N. Sharifi-Mood, K. J. Stebe, Capillary assembly of colloids: Interactions on planar and curved interfaces. *Annu. Rev. Conden. Matter Phys.* **9**, 283–305 (2018).
2. W. B. Rogers, W. M. Shih, V. N. Manoharan, Using DNA to program the self-assembly of colloidal nanoparticles and microparticles. *Nat. Rev. Mater.* **1**, 16008 (2016).
3. P. F. Damasceno, M. Engel, S. C. Glotzer, Predictive self-assembly of polyhedra into complex structures. *Science* **337**, 453–457 (2012).
4. U. Agarwal, F. A. Escobedo, Mesophase behaviour of polyhedral particles. *Nat. Mater.* **10**, 230–235 (2011).
5. A. P. Gantapara, J. de Graaf, R. van Roij, M. Dijkstra, Phase diagram and structural diversity of a family of truncated cubes: Degenerate close-packed structures and vacancy-rich states. *Phys. Rev. Lett.* **111**, 015501 (2013).
6. E. Auyeung *et al.*, DNA-mediated nanoparticle crystallization into Wulff polyhedra. *Nature* **505**, 73–77 (2014).
7. D. Nykypanchuk, M. M. Maye, D. Van Der Lelie, O. Gang, DNA-guided crystallization of colloidal nanoparticles. *Nature* **451**, 549–552 (2008).
8. P. L. Biancaniello, A. J. Kim, J. C. Crocker, Colloidal interactions and self-assembly using DNA hybridization. *Phys. Rev. Lett.* **94**, 058302 (2005).
9. A. P. Alivisatos *et al.*, Organization of 'nanocrystal molecules' using DNA. *Nature* **382**, 609–611 (1996).
10. M.-P. Valignat, O. Theodoly, J. C. Crocker, W. B.Russel, P. M. Chaikin, Reversible self-assembly and directed assembly of DNA-linked micrometer-sized colloids. *Proc. Natl. Acad. Sci. U.S.A.* **102**, 4225–4229 (2005).
11. Y. Wang *et al.*, Crystallization of DNA-coated colloids. *Nat. Commun.* **6**, 7253 (2015).
12. S. E. Seo, M. Girard, M. O. de la Cruz, C. A. Mirkin, Non-equilibrium anisotropic colloidal single crystal growth with DNA. *Nat. Commun.* **9**, 4558 (2018).
13. P. W. K. Rothemund, Folding DNA to create nanoscale shapes and patterns. *Nature* **440**, 297–302 (2006).
14. L. L. Ong *et al.*, Programmable self-assembly of three-dimensional nanostructures from 10,000 unique components. *Nature* **552**, 72–77 (2017).
15. S. M. Douglas *et al.*, Self-assembly of DNA into nanoscale three-dimensional shapes. *Nature* **459**, 414–418 (2009).
16. E. Winfree, F. Liu, L. A. Wenzler, N. C. Seeman, Design and self-assembly of two-dimensional DNA crystals. *Nature* **394**, 539–544 (1998).
17. D. Han *et al.*, DNA origami with complex curvatures in three-dimensional space. *Science* **332**, 342–346 (2011).
18. A. Gopinath, E. Miyazono, A. Faraon, P. W. K. Rothemund, Engineering and mapping nanocavity emission via precision placement of DNA origami. *Nature* **535**, 401–405 (2016).
19. H. Lin *et al.*, Clathrate colloidal crystals. *Science* **355**, 931–935 (2017).
20. W. B. Russel, P. M. Chaikin, J. Zhu, W. V. Meyer, R. Rogers, Dendritic growth of hard sphere crystals. *Langmuir* **13**, 3871–3881 (1997).
21. J. Gong *et al.*, Shape-dependent ordering of gold nanocrystals into large-scale superlattices. *Nat. Commun.* **8**, 14038 (2017).
22. M. Boncheva *et al.*, Magnetic self-assembly of three-dimensional surfaces from planar sheets. *Proc. Natl. Acad. Sci. U.S.A.* **102**, 3924–3929 (2005).
23. J. Stambaugh, K. Van Workum, J. F. Douglas, W. Losert, Polymerization transitions in two-dimensional systems of dipolar spheres. *Phys. Rev. E.* **72**, 031301 (2005).
24. A. Papadopoulou, J. Laucks, S. Tibbits, From self-assembly to evolutionary structures. *Archit. Des.* **87**, 28–37 (2017).
25. Y. Wang *et al.*, Colloids with valence and specific directional bonding. *Nature* **491**, 51–55 (2012).
26. S. W. Prescott, M. J. Ballard, E. Rizzardo, R. G. Gilbert, Successful use of raft techniques in seeded emulsion polymerization of styrene: Living character, raft agent transport, and rate of polymerization. *Macromolecules* **35**, 5417–5425 (2002).
27. R. J. Owen, L. R. Hill, S. P. Lapage, Determination of DNA base compositions from melting profiles in dilute buffers. *Biopolymers* **7**, 503–516 (1969).
28. K. J. Breslauer, R. Frank, H. Blöcker, L. A. Marky, Predicting DNA duplex stability from the base sequence. *Proc. Natl. Acad. Sci. U.S.A.* **83**, 3746–3750 (1986).
29. I. I. Cisse, H. Kim, T. Ha, A rule of seven in Watson-Crick base-pairing of mismatched sequences. *Nat. Struct. Mol. Biol.* **19**, 623–627 (2012).
30. D. Y. Zhang, G. Seelig, Dynamic DNA nanotechnology using strand-displacement reactions. *Nat. Chem.* **3**, 103–113 (2011).
31. M. N. Stojanovic, T. E. Mitchell, D. Stefanovic, Deoxyribozyme-based logic gates. *J. Am. Chem. Soc.* **124**, 3555–3561 (2002).
32. S. M. Douglas, I. Bachelet, G. M. Church, A logic-gated nanorobot for targeted transport of molecular payloads. *Science* **335**, 831–834 (2012).
33. Y. Kim, H. Yuk, R. Zhao, S. A. Chester, X. Zhao, Printing ferromagnetic domains for untethered fast-transforming soft materials. *Nature* **558**, 274–279 (2018).
34. W. Hu, G. Z. Lum, M. Mastrangeli, M. Sitti, Small-scale soft-bodied robot with multimodal locomotion. *Nature* **554**, 81–85 (2018).
35. T. Xu, J. Zhang, M. Salehizadeh, O. Onaizah, E. Diller, Millimeter-scale flexible robots with programmable three-dimensional magnetization and motions. *Sci. Robot.* **4**, eaav4494 (2019).
36. M. H. Kryder *et al.*, Heat assisted magnetic recording. *Proc. IEEE* **96**, 1810–1835 (2008).
37. S. N. Piramanayagam, Perpendicular recording media for hard disk drives. *J. Appl. Phys.* **102**, 011301 (2007).
38. X. Ye *et al.*, Competition of shape and interaction patchiness for self-assembling nanoplates. *Nat. Chem.* **5**, 466–473 (2013).
39. D. Kleshchanok, P. R. Lang, Steric repulsion by adsorbed polymer layers studied with total internal reflection microscopy. *Langmuir* **23**, 4332–4339 (2007).
40. P. Auroy, L. Auvray, L. Leger, Silica particles stabilized by long grafted polymer chains: From electrostatic to steric repulsion. *J. Colloid Interface Sci.* **150**, 187–194 (1992).
41. P. Jenkins, M. Snowden, Depletion flocculation in colloidal dispersions. *Adv. Colloid Interface Sci.* **68**, 57–96 (1996).
42. Y. Mao, M. E. Cates, H. N. W. Lekkerkerker, Depletion force in colloidal systems. *Phys. A Stat. Mech. Appl.* **222**, 10–24 (1995).
43. K. J. Dorsey *et al.*, Atomic layer deposition for membranes, metamaterials, and mechanisms. *Adv. Mater.* **31**, 1901944 (2019).